Signal Processing 132 (2017) 77–84

Contents lists available at ScienceDirect

Signal Processing

journal homepage: www.elsevier.com/locate/sigpro

Scale invariants from Gaussian–Hermite moments

Bo Yang[a], Jitka Kostková[b], Jan Flusser[b,*], Tomáš Suk[b]

[a] School of Automation, Northwestern Polytechnical University, 127 West Youyi Road, 710 072 Xi'an Shaanxi, PR China
[b] Institute of Information Theory and Automation of the CAS, Pod Vodárenskou věží4, 182 08 Prague 8, Czech Republic

ARTICLE INFO

Keywords:
Scale invariants
Gaussian–Hermite moments
Variable modulation
Normalization
Zernike moments

ABSTRACT

Invariants to image scaling composed of Gaussian–Hermite moments are introduced in this paper for the first time. To achieve the invariance, we propose to modulate the Gaussian–Hermite polynomial basis using variable parameter σ, the value of which depends on the input image. The scaling invariance property can be coupled with the rotation invariance presented earlier. This approach is applicable in 2D as well as in 3D and provides very good numerical stability, as demonstrated by several experiments on real data.

1. Introduction

Image descriptors, which are invariant with respect to certain group of coordinate transformations, have been a topic of much recent research in image analysis. Moment invariants form probably the largest class of such kind of features [1,2]. The research on moment invariants has been focused into two main directions. The first one is about looking for the "best" (in some sense) polynomial basis, i.e. the best set of moments the invariants are composed of. The criteria are usually the numerical stability, discrimination power, and computing complexity of the moments. The second direction is designing invariants w.r.t. new transformation groups.

In the moment-related literature, we may find endless discussion and a number of comparative experiments about what type of moments provides the maximum separability of objects, maximum robustness, and requires minimum computational time. Individual experiments exhibit statistically insignificant results and/or contradict to experiments presented by other authors. Apparently, there is no "optimal" type of moments since the results depend substantially on the particular data. Nevertheless, most authors agree that for practical applications where the moments are supposed to be computed on mid-size or large images, we should focus on orthogonal (OG) polynomials and orthogonal moments. Comparing to geometric moments, which are suitable for theoretic considerations because of their simplicity, OG moments are numerically more stable.

Among various orthogonal moments [3–9], Gaussian–Hermite (GH) moments play a special role. The GH polynomials and moments were introduced into the image analysis area by Shen [10,11] and were proved to be very robust w.r.t. additive noise comparing to other common moments, which is a remarkable advantage [12,13]. They were employed in several successful applications, such as in detection of moving objects in a video [14], in licence plate recognition [15], in image registration as landmark descriptors [16], in fingerprint classification [17], in face recognition [18,19], and as directional feature extractors [20]. GH polynomials are orthogonal on a rectangular area, which is suitable when working with digital images. The polynomials orthogonal on a disk, such as Zernike, radial Chebyshev, and similar polynomials, require polar resampling of the image, which not only increases the computation time but also leads to the loss of precision. Generally, it is difficult to construct rotation invariants, which are important for object recognition, from moments orthogonal on a rectangle (on the contrary, the moments orthogonal on a disk can be made rotation-invariant easily). The GH moments are the only moments orthogonal on a rectangle which offer a possibility of an easy and efficient design of rotation invariants. This is guaranteed by the *Yang's Theorem*, which holds in 2D [9,21,22] as well as in 3D [23].

The main drawback of using the GH moments for object recognition is a (somehow surprising) fact, that their invariance w.r.t. scaling has not been discovered yet. In case of other common moments, the scaling invariance can be achieved easily by normalizing the moments by an object area or by a mean graylevel of the image. We show in the paper why this approach fails in case of the GH moments.

In this paper, we present a novel method how to make the GH moments invariant to image scaling. This idea works in an arbitrary number of dimensions. The new normalized GH moments can be used individually or can be substituted into the general formulas for rotation GH invariants proposed in [22]. The substitution does not violate the rotation invariance and yields rotation-scaling invariants. In this sense, this paper can be viewed as a generalization of our recent work [9,22] published in this journal.

* Corresponding author.
E-mail addresses: bo.yang@hotmail.fr (B. Yang), kostkova@utia.cas.cz (J. Kostková), flusser@utia.cas.cz (J. Flusser), suk@utia.cas.cz (T. Suk).

http://dx.doi.org/10.1016/j.sigpro.2016.09.013
Received 25 June 2016; Received in revised form 29 August 2016; Accepted 17 September 2016
Available online 01 October 2016
0165-1684/ © 2016 Elsevier B.V. All rights reserved.

The paper is organized as follows. In the next section, we briefly recall the basics about the GH polynomials and moments. We show in Section 3 why the common approach to moment normalization w.r.t. scaling cannot work for the GH moments. Section 4 presents the new idea of designing scale invariants by variable modulation. In Section 5 we explain how to achieve simultaneous invariants to scaling, rotation and contrast changes. Finally, in Section 6, we illustrate the performance of the proposed invariants by experiments on real 2D and 3D images.

2. Recalling Gaussian–Hermite polynomials and moments

Hermite polynomial of the n-th degree is defined as [24]

$$H_n(x) = (-1)^n e^{x^2} \frac{\mathrm{d}^n}{\mathrm{d}x^n} e^{-x^2}. \tag{1}$$

The three-term recurrence relation, which is used for fast and stable evaluation of H_n, is

$$H_0(x) = 1,\ H_1(x) = 2x,\ H_n(x) = 2xH_{n-1}(x) - 2(n-1)H_{n-2}(x). \tag{2}$$

General explicit expression of the Hermite polynomials is

$$H_n(x) = n! \sum_{k=0}^{[n/2]} \frac{(-1)^k (2x)^{n-2k}}{k!(n-2k)!},$$

but it is not appropriate for numerical calculations.

Hermite polynomials are orthogonal on $(-\infty, \infty)$ with the weight $w(x) = e^{-x^2}$

$$\int_{-\infty}^{\infty} e^{-x^2} H_n(x) H_m(x) \mathrm{d}x = n! 2^n \sqrt{\pi} \delta_{nm}. \tag{3}$$

If they were not modulated, they would have a high dynamic range and poor localization, which would make them difficult to use directly for image description. To overcome this, we modulate Hermite polynomials with a Gaussian function and scale them. This normalization yields *Gaussian–Hermite polynomials*

$$\widehat{H}_n(x, \sigma) = e^{-\frac{x^2}{2\sigma^2}} \frac{1}{\sqrt{n! 2^n \sigma \sqrt{\pi}}} H_n(x/\sigma) \tag{4}$$

which are not only orthogonal but also orthonormal

$$\int_{-\infty}^{\infty} \widehat{H}_n(x, \sigma) \widehat{H}_m(x, \sigma) \mathrm{d}x = \delta_{nm}. \tag{5}$$

As can be seen in Fig. 1, the GH polynomials have the range of values inside $(-1, 1)$. Even if they are formally defined on $(-\infty, \infty)$, they are effectively localized in a small neighborhood of the origin controlled by the parameter σ.

1D Gaussian–Hermite moment of order p of function f is defined as

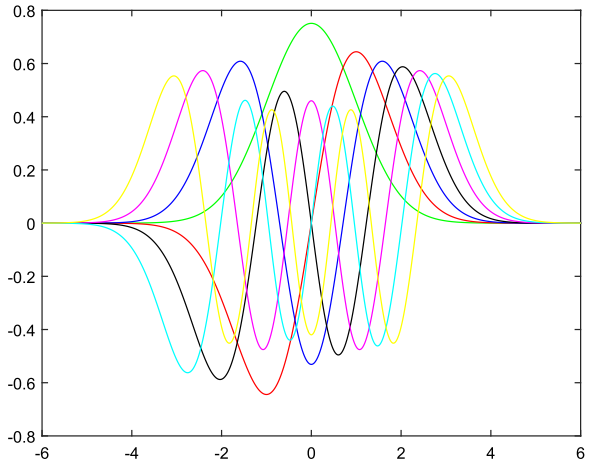

Fig. 1. The graphs of the Gaussian–Hermite polynomials up to degree 6 with $\sigma = 1$.

$$\widehat{\eta}_p = \int_{-\infty}^{\infty} \widehat{H}_p(x, \sigma) f(x) \mathrm{d}x. \tag{6}$$

This definition can be readily extended into an arbitrary number of dimensions N as

$$\widehat{\eta}_{p_1,\ldots,p_N} = \int_{-\infty}^{\infty} \cdots \int_{-\infty}^{\infty} f(x_1,\ldots,x_N) \prod_{k=1}^{N} \widehat{H}_{p_k}(x_k, \sigma) \mathrm{d}x_k. \tag{7}$$

3. Gaussian–Hermite moments under scaling

Let us investigate how the GH moments are transformed under scaling $x' = sx$, where s is a positive scaling factor. We show this in 1D first. For the sake of simplicity, we work with the non-coefficient form of GH polynomials

$$H_n(x, \sigma) = e^{-\frac{x^2}{2\sigma^2}} H_n(x/\sigma) \tag{8}$$

and corresponding non-coefficient GH moments

$$\eta_p = \int_{-\infty}^{\infty} H_p(x, \sigma) f(x) \mathrm{d}x. \tag{9}$$

Dropping the multiplicative factor only violates the orthonormality but has no impact on the design of the invariants.

The GH moments are transformed under scaling as

$$\eta_{'p} = \int_{-\infty}^{\infty} H_p(x, \sigma) f(x/s) \mathrm{d}x = \int_{-\infty}^{\infty} H_p(sx, \sigma) f(x) s \mathrm{d}x = s \int_{-\infty}^{\infty} H_p(x, \sigma/s) f(x) \mathrm{d}x. \tag{10}$$

It is not possible to eliminate the scaling factor from the argument of H_p. In other words, we cannot express the moment after the scaling η_{p}' in terms of the original moments $\eta_0,\ldots,\eta_p$. Let us recall that such expression is the key to a successful design of the invariants. In case of geometric moments

$$m_p = \int_{-\infty}^{\infty} x^p f(x) \mathrm{d}x \tag{11}$$

it holds

$$m_{'p} = s^{p+1} m_p \tag{12}$$

and the scaling factor can be cancelled by normalization m_p/m_0^{p+1}. The same idea works for all common moments, but as we have seen it cannot be applied to the GH moments.

4. Scale invariants of Gaussian–Hermite moments

The main difficulty in designing GH invariants to scaling arises from the fact that the parameter σ is fixed. To overcome this, we need to replace the constant σ in the definition of GH polynomials by variable $\sigma(f)$, which depends on the function f the moments are calculated of and which "adapts" itself whenever f is scaled. Under the scaling, it should be transformed as

$$\sigma(f') = s\sigma(f). \tag{13}$$

There are many possible choices of such $\sigma(f)$. The simplest one (which is also the most robust) is

$$\sigma(f) = \sigma_0 m_0, \tag{14}$$

where m_0 is the zero-order moment of f and σ_0 is a positive constant which controls the modulation. This choice fulfills the requirement (13).

Now let us show how the GH moments with this variable modulation (we denote them $\tilde{\eta}_p$) are transformed under scaling

$$\tilde{\eta}'_p = \int_{-\infty}^{\infty} H_p(x, \sigma(f'))f(x/s)\mathrm{d}x = = \int_{-\infty}^{\infty} H_p(sx, s\sigma(f))f(x)s\mathrm{d}x = = s\int_{-\infty}^{\infty} H_p(x, \sigma(f))f(x)\mathrm{d}x = s\tilde{\eta}_p. \quad (15)$$

Considering that $m_{/0} = sm_0$, we define *scale-invariant GH moments* as

$$\nu_p = \tilde{\eta}_p/m_0 \quad (16)$$

(the normalization with m_0 is the simplest one among many other possible normalizations).

The extension to N dimensions is easy thanks to the separability of multidimensional GH polynomials. We assume uniform scaling $x_{/k} = sx_k$ for all $k = 1,\ldots,N$. If we set

$$\sigma(f) = \sigma_0 \sqrt[N]{m_{00\ldots0}}, \quad (17)$$

we get the desirable relation

$$\sigma(f') = \sigma_0 \sqrt[N]{s^N m_{00\ldots0}} = s\sigma(f). \quad (18)$$

Hence, the multidimensional GH moments are transformed under scaling as

$$\tilde{\eta}'_{p_1,\ldots,p_N} = \int_{-\infty}^{\infty}\cdots\int_{-\infty}^{\infty} f\left(x_1/s,\ldots,x_N/s\right)\prod_{k=1}^{N} H_{p_k}\left(x_k, \sigma\left(f'\right)\right)\mathrm{d}x_k = s^N\int_{-\infty}^{\infty}\cdots\int_{-\infty}^{\infty} f\left(x_1,\ldots,x_N\right)\prod_{k=1}^{N} H_{p_k}\left(sx_k, s\sigma(f)\right)\mathrm{d}x_k = s^N\tilde{\eta}_{p_1,\ldots,p_N}. \quad (19)$$

As in 1D, the normalization

$$\nu_{p_1,\ldots,p_N} = \tilde{\eta}_{p_1,\ldots,p_N}/m_{00\ldots0} \quad (20)$$

yields invariants to scaling for any indexes $p_1,\ldots,p_N$.

In the proposed normalization, the only user-defined parameter is σ_0, which is an initialization parameter that is the same on all scales. Its choice has nothing to do with the scaling invariance; the scale normalization works well for any $\sigma_0 > 0$. The choice of σ_0 influences the modulation of Hermite polynomials and the suppression of boundary regions of the image. There is no general criterion for an optimal selection of σ_0 and their recommended choice was derived empirically. At the initial scale (i.e. for a database image) we have in the 2D case $\sigma(f) = \sigma_0\sqrt{m_{00}}$ and the choice of σ_0 may be deduced from the rules derived earlier for the choice of (fixed) $\sigma(f)$. An empirical rule which optimizes the reconstruction abilities of the GH moments was proposed in [16]. Since the invariants proposed in this paper should serve for recognition rather than reconstruction of the image, we used a simpler rule. The value of σ_0 should be selected such that on the initial scale $\sigma_0\sqrt{m_{00}}$ is between 0.3 and 1.5 multiple of the image size, depending on how much we want to suppress the boundary regions.

5. Combining scale, rotation, and contrast invariants

For most of practical applications in 2D and 3D, the simultaneous invariance w.r.t. scaling, rotation and translation is required. Translation invariance is obvious and can be achieved easily just by shifting the GH polynomials from the coordinate origin to the centroid of the image. Invariants to rotation can be constructed due to the Yang's Theorem (see [9,21] for its 2D version and [23] for the 3D version with complete proofs). The theorem in 2D states that if there exists a rotation invariant of geometric moments $I(m_{p_1q_1}, m_{p_2q_2},\ldots,m_{p_dq_d})$, the same function of the corresponding Gaussian Hermite moments $I(\eta_{p_1q_1}, \eta_{p_2q_2},\ldots,\eta_{p_dq_d})$ is also a rotation invariant. The statement is the same in 3D and holds both for the non-coefficient as well as coefficient forms of the GH moments. Explicit general forms of rotation invariants of arbitrary-order GH moments, that were designed using the Yang's Theorem, can be found in [22].

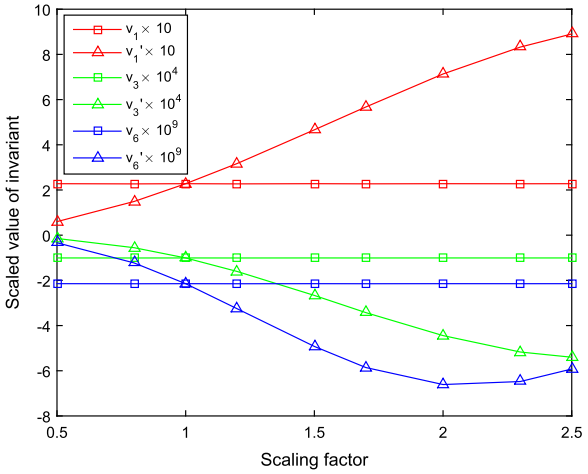

Fig. 2. Sample GH scale invariants $\nu_1 = \nu_{5,5}$, $\nu_3 = \nu_{7,8}$, and $\nu_6 = \nu_{11,12}$ calculated over nine different image scales. They exhibit almost perfect invariance. The normalized moments of the same indexes are denoted as ν'_1, ν'_3, and ν'_6. They change significantly as the image has been scaled. Note that $\nu_k = \nu'_k$ if s=1.

Table 1
Relative errors of the scaling invariants (%).

	υ_1	υ_3	υ_6
GH with $\sigma(f)$	0.14	0.06	0.06
GH with fixed σ	146	223	133
ZM with mapping	0.17	0.42	0.28

The Yang's Theorem holds well even for the scale-normalized GH moments ν_{pq}, because the normalization by m_{00}, which itself is a rotation invariant, does not violate the invariance property. Substituting them into the formulas for rotation invariants, we obtain invariants of the GH moments to scaling and rotation.

In some applications, additional invariance to contrast stretching may be required. The underlaying model in 2D is

$$f'(x, y) = cf(x/s, y/s). \quad (21)$$

To eliminate the contrast parameter c from $\sigma(f)$, we choose

$$\sigma(f) = \sigma_0\sqrt{(m_{20} + m_{02})/m_{00}} \quad (22)$$

(other choices using higher-order moments are also possible). Then it holds $\sigma(f') = s\sigma(f)$ and, consequently, $\tilde{\eta}_{/pq} = cs^2\tilde{\eta}_{pq}$. Normalization with m_{00} leads to scale-contrast invariants, which can again be substituted into the formulas of rotation invariants. The same can be done in 3D with the setting

$$\sigma(f) = \sigma_0\sqrt{(m_{200} + m_{020} + m_{002})/m_{000}}. \quad (23)$$

6. Numerical experiments

The goal of the experiments is namely to demonstrate that the variable modulation actually yields scale invariant GH moments, unlike the constant modulation. We also show the possibility of coupling scaling and rotation invariance together. We do not compare the scale-invariant GH moments to geometric moments. Exhaustive tests of numerical properties of the GH moments with constant modulation and of their recognition and reconstruction power were already performed in [22,23] and showed the superiority of the GH moments over the geometric moments. Introducing the variable modulation does not change these advantageous properties.

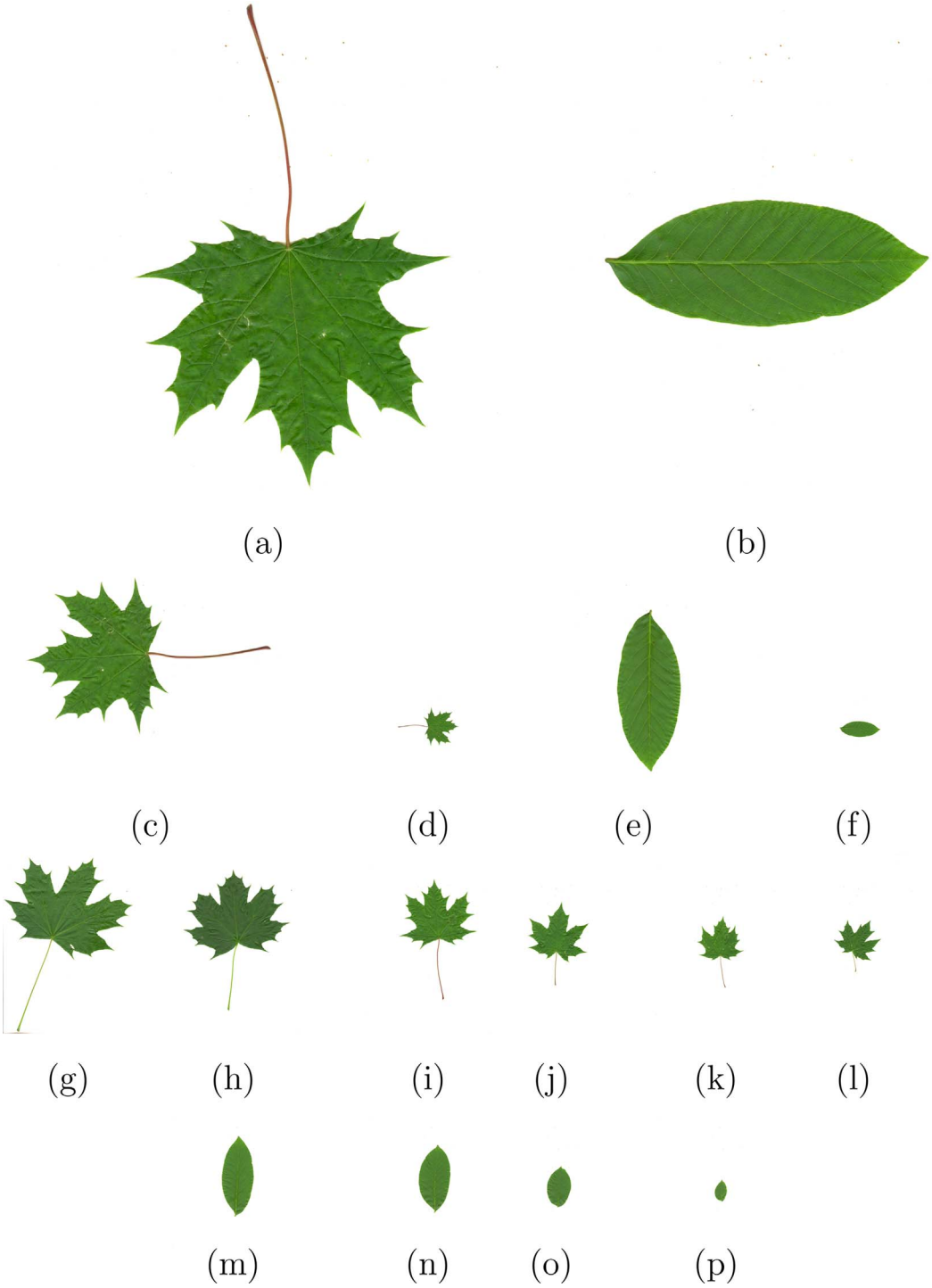

Fig. 3. The leaves used in the experiment: (a), (c), (d), (g), (h), (i), (j), (k), (l) *Acer platanoides*, (b), (e), (f), (m), (n), (o), (p) *Juglans regia*. The leaves (g)–(p) were scanned in the resolution 300 dpi, (a), (b) 1200 dpi, (c), (e) 600 dpi and (d), (f) 150 dpi, respectively.

6.1. 2D images with artificial scaling

The first experiment was done on the image which was scaled artificially by means of bilinear interpolation. Computer-generated scaling allowed us to control the scaling parameter, to evaluate the results quantitatively, and to eliminate any other unwanted factors. We used the famous "Cameraman" 512×512 graylevel image at nine different scales: 0.5, 0.8, 1.0, 1.2, 1.5, 1.7, 2.0, 2.3, and 2.5.

We calculated scale invariants $\nu_{pq} = \tilde{\eta}_{pq}/m_{00}$ with variable $\sigma(f)$, which were defined in Eq. (20), up to the order 20. According to the recommendation given in Section 4, we set $\sigma_0 = 0.0042$, which ensures that the Gaussian function with $\sigma(f)$ reasonably covers the image. All invariants ν_{PQ} were perfectly stable over the whole range of scales, the only errors were caused by resampling and numerical inaccuracies. Most of the mean relative errors were far below 1%.

To illustrate that the variable $\sigma(f)$ actually makes a substantial difference from the fixed σ, we repeated this experiment with normalized moments η_{pq}/m_{00}. To make the experiments comparable, we set $\sigma = \sigma(f_1)$, where f_1 means the image at the original scale s=1 and $\sigma(f_1)$ has been calculated in the first experiment. In the current experiment, σ stays constant over all image scales. The normalized moments do not exhibit any invariant property. They change significantly, yielding the

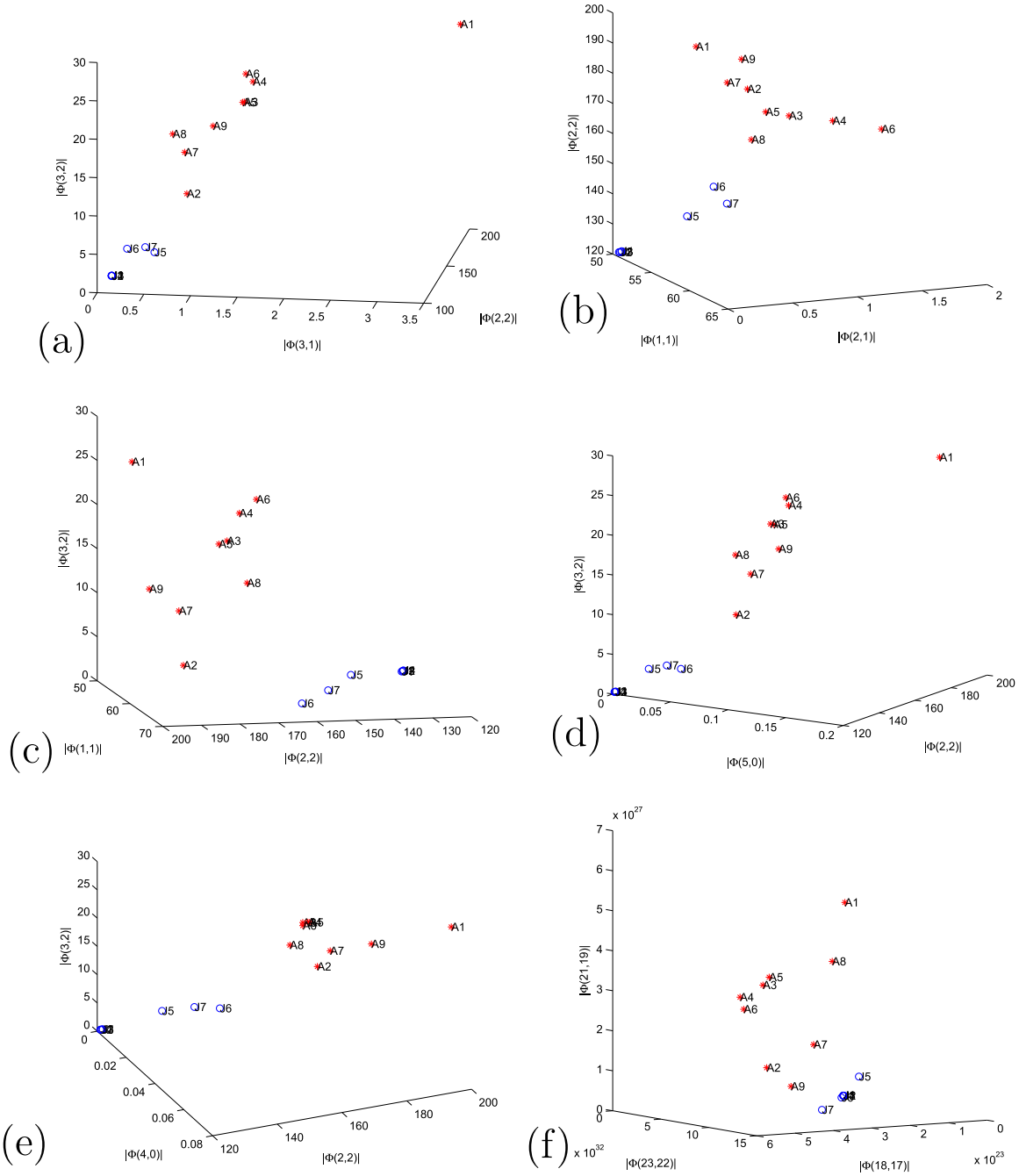

Fig. 4. The leaves represented by rotation-scale GH invariants, *Acer platanoides* (red asterisk) and *Juglans regia* (blue circle). The magnitudes of the invariants are used for visualization purposes. The separability of the two species is evident. (For interpretation of the references to color in this figure caption, the reader is referred to the web version of this paper.)

mean relative errors over 100%. The behavior of three sample invariants and three normalized moments with constant σ is shown in Fig. 2; the relative errors can be seen in Table 1, lines one and two.

We repeated this experiment with five other well-known benchmark images (Baboon, Barbara, Goldhill, Boat, Peppers, and Lena) with exactly the same conclusions.

Finally, we compared the proposed GH invariants with scale-invariant Zernike moments. Zernike moments (ZMs) [3] have become very popular in image analysis and have found numerous applications. Their main advantage comes from the fact that they are orthogonal on a unit disk and their magnitude does not change under an image rotation (the family of moments with this rotation property contains several similar "radial" moments such as Pseudo–Zernike, Fourier–Mellin [25], Jacobi–Fourier [26–28], Chebyshev–Fourier [29], and others). This property ensures a theoretically easy construction of rotation invariants [5]. Zernike moments, as well as other radial moments, are not inherently invariant to scaling. However, the image must be mapped into the unit disk before the Zernike moments can be calculated. This mapping implicitly provides the scaling invariance. Using the same "Cameraman" image scaled as above, we calculated Zernike moments and compared them to the corresponding GH moments[1] (see Table 1, line three). It can be observed, that the ZMs

[1] The correspondence between ZMs and GHs is not straightforward because the second index of the Zernike moment expresses an angular repetition factor while both indices of the GH moments are the degrees of the polynomials. Reasonable pairs to be

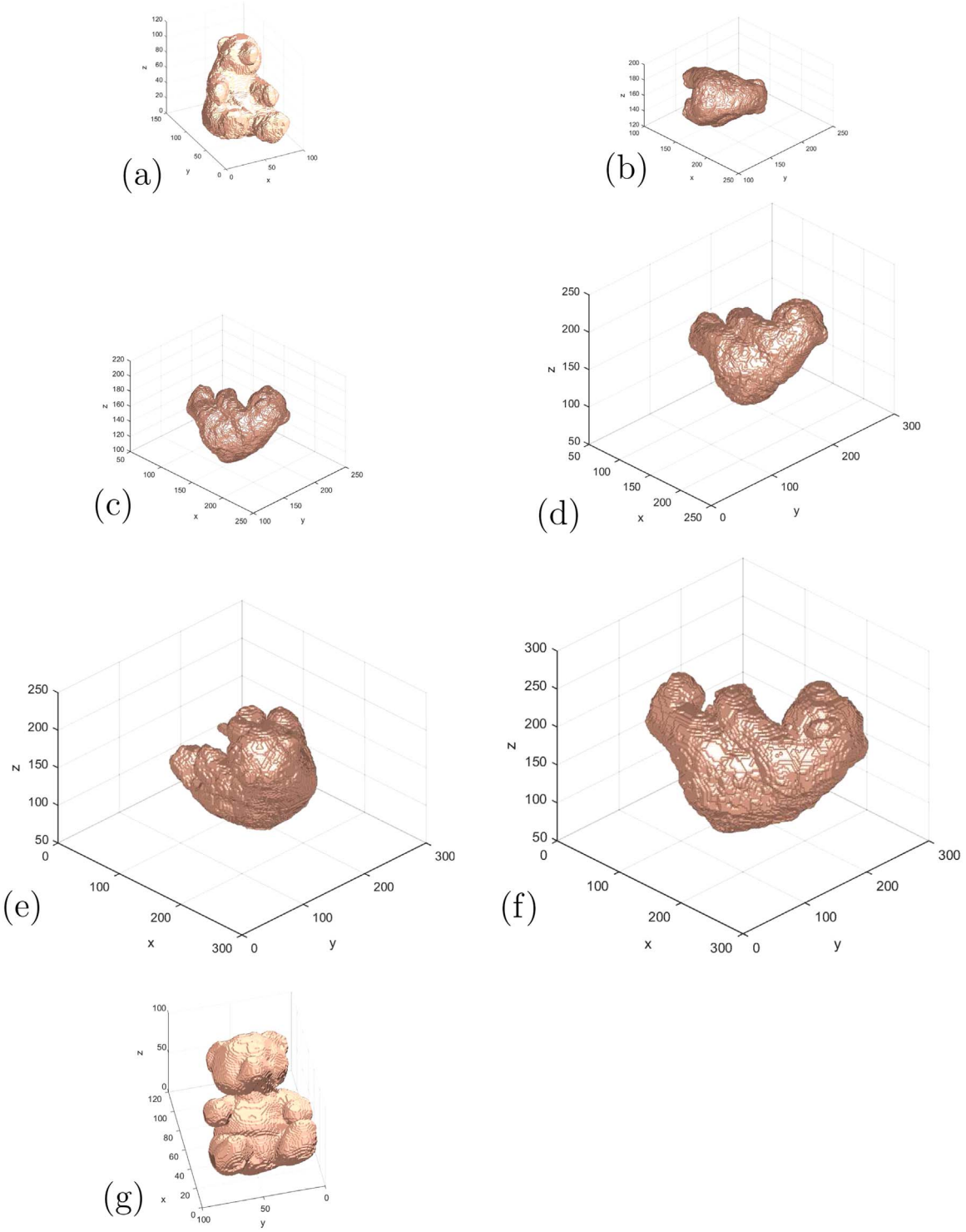

Fig. 5. (a)–(f) Teddy bear No. 1 in six different scales and orientations, (g) Teddy bear No. 2.

actually exhibit the scaling invariance but their numerical accuracy is slightly worse than that of the GH moments with variable $\sigma(f)$. The main reason for this effect is that the calculation of ZMs requires image resampling into polar coordinates. Although there exist alternative algorithms that seemingly do not perform any resampling, they cannot overcome the principle necessity of working in a polar raster which always generates numerical errors. The errors induced by the polar raster in ZM calculation were analyzed in detail by Pawlak in [30]. Another factor which could also contribute to the errors is that the zeros of the GH polynomials are distributed more evenly than those of the Zernike polynomials. This comparison shows the prominent position of the GH moments, their orthogonality on a rectangular grid yields very good numerical stability while the Yang's theorem and the proposed variable normalization provide an easy construction of rotation and scaling invariants.

(*footnote continued*)
compared are $GH_{p,q}$ and $ZM_{p+q,p-q}$.

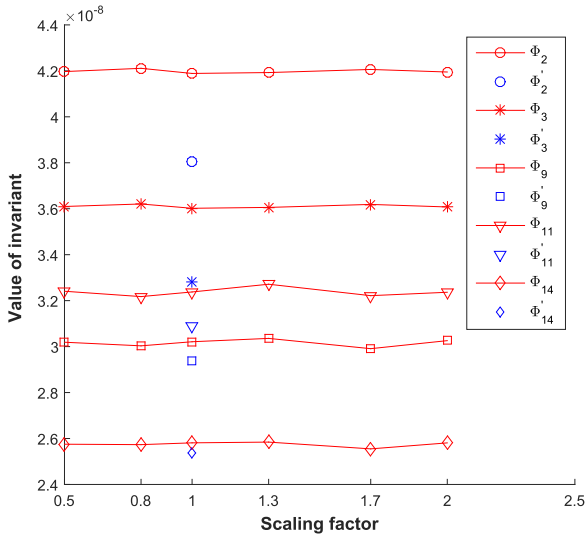

Fig. 6. Sample GH scale-rotation 3D invariants Φ_2, Φ_3, Φ_9, Φ_{11}, and Φ_{14} of the teddy bears. The corresponding mean relative errors of the invariants over six instances are 0.2%, 0.2%, 0.5%, 0.6%, and 0.4%, respectively. Note that except Φ_{14}, the values of Teddy bear No. 2 (denoted as Φ') are significantly different from those of Teddy bear No. 1.

6.2. 2D images with real scaling and rotation

This experiment demonstrates the behavior of the invariants under a real scaling coupled with real rotations. In addition to the invariance, we also demonstrate the discriminability between two different shape classes. The test images came from the MEW database [31], the largest leaf database of Central European wood species which contains the leaves of all domestic and most of the imported trees and shrubs growing in the Central Europe (about 15,000 leaf items, representing 201 species).

The leaves of the same species often differ from each other significantly by the size, shape, color and texture. Their images in the database may have various orientation as the leaves were not scanned in a normalized position, some of them were even scanned upside down. The spatial resolution of the scanner varies as well. All these variances should be covered by the invariant properties. Within-class shape variations range from slight to significant. Of course, the invariants cannot be perfectly stable w.r.t. these shape variations but should exhibit certain degree of robustness. The goal of this experiment is to study the within-class deviations of the GH scale-rotation invariants. We do not aim to build up a new leaf recognition system based on the GH moments. As explained in [32], a successful system should combine features of various kinds together. We only want to test the proposed GH scale invariants in a real environment.

We chose two sample classes, the Norway maple (*Acer platanoides*) and the English walnut (*Juglans regia*), that actually contain leaves of various shape, size, orientation, and scanner resolution (in Fig. 3, subfigures (a), (c), (d), and (i) are different scans of the same leaf, similarly as (b), (e), (f), and (m)). To remove color and texture variations, we thresholded all leaves and worked with binary images only. For each leaf we calculated scale-rotation GH invariants obtained by substitution of scale invariants ν_{pq} (20) into the formulas of 2D rotation invariants derived in [22]. Although the invariance is not perfect, the two species are well separated in the feature space even if we consider a few invariants only. One can see some examples of subspaces of three invariants in Fig. 4. If we increase the dimension and consider more invariants together, the separability further improves.

6.3. 3D objects

Public databases of 3D shapes such as the Princeton Shape Benchmark (PSB) [33] consist mostly of CAD models of simplified objects, which are stored in a single scale and orientation. They seldom contain images of real objects. The tests on noise-free ideal models, the scaling of which would have to be generated artificially, are neither challenging nor convincing. This is why we decided to perform the experiment on real objects with actually different positions in the space.

We scanned a teddy bear by means of the Kinect device. Then we repeated this process five times with different orientations of the teddy bear in the space. Hence, we obtained six complete scans differing from each other by rotation and also slightly by scale and by quality of the details. To increase the variation of size, we scaled the scans by the factors 0.5, 0.8, 1.0, 1.3, 1.7, and 2.0, respectively (see Fig. 5(a)–(f)). For a comparison we also scanned another teddy bear, which is similar to the first one at the first sight but is actually of a different shape (see Fig. 5(g)). The second teddy bear was scanned only once. We chose teddy bears as test objects because their surface, covered by coat, introduced random errors into the scanning process, which made the experiment more challenging. The Kinect software produces a triangulated representation of the object surface. To calculate the moments, we converted each teddy bear figure into 3D volumetric representation. The size at the largest scale was approximately $300 \times 300 \times 300$ voxels.

To construct GH scale-rotation 3D invariants, we again used the substitution principle. In 3D, however, the structure of the set of rotation invariants is more rich than in 2D. There exist 1185 irreducible rotation invariants up to the order 16 constructed from geometric moments (their complete list is available in [34], the relevant theory can be best found in [2,35]). We substituted the scale invariants ν_{pqr} with variable $\sigma(f)$ (20) into all of them and evaluated them on all six instances of the Teddy bear No. 1. The relative error of the invariants slightly increases as the moment order increases but in most cases it has been kept in a reasonable interval, except 14 invariants, all others have relative error less than 6% (relative errors of those 14 invariants are high because their absolute values are very close to zero). The behavior of five sample invariants (we denote them as Φ_2, Φ_3, Φ_9, Φ_{11}, and Φ_{14} to preserve the consistency with the paper [23]) is shown in Fig. 6. We can see that the values of the invariants, calculated on Teddy bear No. 1, stay almost perfectly constant over all orientations and scales. Slight variations, leading to mean relative errors from 0.2% to 0.6%, are caused by measurement errors when the object has been scanned. We can also see that the values of Teddy bear No. 2 are significantly different (except Φ_{14}), which illustrates the recognition power of the GH invariants.

7. Conclusion

In this paper we extended the theory of Gaussian–Hermite moment invariants, which was introduced originally in [9,21–23] for rotation and translation, also to scaling transformation. We showed the scaling invariance cannot be achieved when using traditional definition of the GH moments with a constant modulation. To overcome this, we proposed the idea of a variable modulation by $\sigma(f)$. As proved theoretically as well as by the experiments, this idea works in any dimension and even allows to combine the scaling and rotation invariance together. The main advantage of the proposed scale and rotation-scale GH invariants is their numerical stability.

Acknowledgments

This work was supported by the National Natural Science Foundation of China (Grant No. 61502389), by the Fundamental Research Funds for the Central Universities (Grant No. 3102015ZY047), by the Czech Science Foundation (Grant No. GA15-16928S), and by the Grant Agency of the Czech Technical University (Grant No. SGS15/214/OHK4/3T/14).

References

[1] J. Flusser, T. Suk, B. Zitová, Moments and Moment Invariants in Pattern Recognition, Wiley, Chichester, 2009.
[2] J. Flusser, T. Suk, B. Zitová, 2D and 3D Image Analysis by Moments, Wiley, Chichester, U.K, 2016.
[3] M.R. Teague, Image analysis via the general theory of moments, J. Opt. Soc. Am. 70 (8) (1980) 920–930.
[4] A. Khotanzad, Y.H. Hong, Invariant image recognition by Zernike moments, IEEE Trans. Pattern Anal. Mach. Intell. 12 (5) (1990) 489–497.
[5] Å Wallin, O. Kübler, Complete sets of complex Zernike moment invariants and the role of the pseudoinvariants, IEEE Trans. Pattern Anal. Mach. Intell. 17 (11) (1995) 1106–1110.
[6] K.M. Hosny, New set of rotationally Legendre moment invariants, Int. J. Electr. Electron. Eng. 4 (2010) 176–180.
[7] P.-T. Yap, R. Paramesran, S.-H. Ong, Image analysis by Krawtchouk moments, IEEE Trans. Image Process. 12 (11) (2003) 1367–1377.
[8] Y.J. Li, Reforming the theory of invariant moments for pattern recognition, Pattern Recognit. 25 (1992) 723–730.
[9] B. Yang, M. Dai, Image analysis by Gaussian–Hermite moments, Signal Process. 91 (2011) 2290–2303.
[10] J. Shen, Orthogonal Gaussian–Hermite moments for image characterization, in: D. P. Casasent (Ed.), Intelligent Robots and Computer Vision XVI: Algorithms, Techniques, Active Vision, and Materials Handling, vol. 3208, SPIE, 1997, pp. 224–233.
[11] J. Shen, W. Shen, D. Shen, On geometric and orthogonal moments, Int. J. Pattern Recognit. Artif. Intell. 14 (7) (2000) 875–894.
[12] L. Wang, Y. Wu, M. Dai, Some aspects of Gaussian–Hermite moments in image analysis, in: L.P. Suresh, S.S. Dash, B.K. Panigrahi (Eds. in:), Proceedings of the Third International Conference on Natural Computation ICNC'07, Advances in Intelligent Systems and Computing, vol. 2, IEEE, 2007, pp. 450–454.
[13] J. Shen, W. Shen, D. Shen, On geometric and orthogonal moments, in: J. Shen, P.S. P. Wang, T. Zhang (Eds.), Multispectral Image Processing and Pattern Recognition, Machine Perception Artificial Intelligence, vol. 44, World Scientific Publishing, Singapore, 2001, pp. 17–36.
[14] Y. Wu, J. Shen, Properties of orthogonal Gaussian–Hermite moments and their applications, EURASIP J. Appl. Signal Process. (4) (2005) 588–599.
[15] X. Ma, R. Pan, L. in: Wang, License plate character recognition based on Gaussian–Hermite moments, in: Proceedings of the Second International Workshop on Education Technology and Computer Science ETCS'10, vol. 3, IEEE, 2010, pp. 11–14.
[16] B. Yang, T. Suk, M. Dai, J. Flusser, 2D and 3D image analysis by Gaussian–Hermite moments, in: G.A. Papakostas (Ed.), Moments and Moment Invariants - Theory and Applications, Science Gate Publishing, Xanthi, Greece, 2014, pp. 143–173.
[17] L. Wang, M. Dai, Application of a new type of singular points in fingerprint classification, Pattern Recognit. Lett. 28 (13) (2007) 1640–1650.
[18] S. Farokhi, U.U. Sheikh, J. Flusser, B. Yang, Near infrared face recognition using Zernike moments and Hermite kernels, Inf. Sci. 316 (2015) 234–245.
[19] N. Belghini, A. Zarghili, J. Kharroubi, 3D face recognition using Gaussian Hermite moments, Int. J. Comput. Appl., Spec. Issue Softw. Eng., Databases Expert Syst. SEDEX 1 (2012) 1–4.
[20] B. Yang, J. Flusser, T. Suk, Steerability of Hermite kernel, Int. J. Pattern Recognit. Artif. Intell. 27 (4) (2013) 1–25.
[21] B. Yang, G. Li, H. Zhang, M. Dai, Rotation and translation invariants of Gaussian–Hermite moments, Pattern Recognit. Lett. 32 (2) (2011) 1283–1298.
[22] B. Yang, J. Flusser, T. Suk, Design of high-order rotation invariants from Gaussian–Hermite moments, Signal Process. 113 (1) (2015) 61–67.
[23] B. Yang, J. Flusser, T. Suk, 3D rotation invariants of Gaussian–Hermite moments, Pattern Recognit. Lett. 54 (1) (2015) 18–26.
[24] C. Hermite, Sur un nouveau développement en série des fonctions, vol. 58, Gauthier-Villars, 1864, (in French).
[25] Y. Sheng, J. Duvernoy, Circular-Fourier-radial-Mellin transform descriptors for pattern recognition, J. Opt. Soc. Am. A 3 (6) (1986) 885–888.
[26] Z. Ping, H. Ren, J. Zou, Y. Sheng, W. Bo, Generic orthogonal moments: Jacobi–Fourier moments for invariant image description, Pattern Recognit. 40 (4) (2007) 1245–1254.
[27] R. Upneja, C. Singh, Fast computation of Jacobi–Fourier moments for invariant image recognition, Pattern Recognit. 48 (5) (2015) 1836–1843.
[28] R. Upneja, Accurate and fast Jacobi-Fourier moments for invariant image recognition, Opt. - Int. J. Light Electron Opt. 127 (19) (2016) 7925–7940.
[29] Z. Ping, R. Wu, Y. Sheng, Image description with Chebyshev–Fourier moments, J. Opt. Soc. Am. A 19 (9) (2002) 1748–1754.
[30] M. Pawlak, Image Analysis by Moments: Reconstruction and Computational Aspects, Oficyna Wydawnicza Politechniki Wrocławskiej, Wrocław, Poland, 2006.
[31] MEW 2012, Download middle european woods, 2014 ⟨http://zoi.utia.cas.cz/node/662⟩.
[32] P. Novotný, T. Suk, Leaf recognition of woody species in central europe, Biosyst. Eng. 115 (4) (2013) 444–452.
[33] P. Shilane, P. Min, M. Kazhdan, T. Funkhouser, Princet. Shape Benchmark (2004) [URL ⟨http://shape.cs.princeton.edu/benchmark/⟩].
[34] DIP, 3D rotation moment invariants, (2011) ⟨http://zoi.utia.cas.cz/3DRotationInvariants⟩.
[35] T. Suk, J. Flusser, Tensor method for constructing 3D moment invariants, in: Computer Analysis of Images and Patterns CAIP'11, Lecture Notes in Computer Science, vol. 6854–6855, Springer, Seville, Spain, 2011, pp. 212–219.